Statistical Modeling of Fingerprint Minutiae

Jianjiang Feng, Anil K. Jain, and Jie Zhou

Abstract

Understanding the probabilistic distribution of fingerprint patterns is of fundamental importance to address many problems in fingerprint recognition, including synthesis, feature extraction, and individuality assessment. Because of the distinctiveness of minutiae and the popularity of minutiae-based representation in Automated Fingerprint Identification Systems (AFIS), fingerprint modeling is often posed in terms of modeling of minutiae patterns. Although several statistical models of minutiae patterns have been proposed in the literature, they have not been subjected to careful validation. In this paper a two-level generative model is proposed to approximate the statistics of fingerprint minutiae patterns. The first level of the model approximates the distribution of orientation field whereas the second level models the distribution of minutiae location and polarity as a marked inhomogeneous Poisson point process. We also propose a new minutiae-based fingerprint reconstruction algorithm which is used to evaluate the proposed minutiae model as well as other models published in the literature. Experimental results show that fingerprints reconstructed from minutiae sets sampled by the proposed model are much more realistic than minutiae simulated by the previous published models. We also show the application of the proposed model in recognizing invalid fingerprint minutiae patterns and using minutia distinctiveness to improve match score computation.

Index Terms

Fingerprint model, synthesis, fingerprint reconstruction, minutiae, spatial statistics, spiral phase, point process.

Jianjiang Feng and Jie Zhou are with the Department of Automation, Tsinghua University, Beijing 100084, China. E-mail: jfeng@tsinghua.edu.cn, jzhou@tsinghua.edu.cn

Anil K. Jain is with the Department of Computer Science and Engineering, Michigan State University, East Lansing, MI-48824, U.S.A. He is also affiliated with the Department of Brain & Cognitive Engineering, Korea University, Seoul, S. Korea. E-mail: jain@cse.msu.edu

I. INTRODUCTION

The friction ridge skin on human fingers forms a flow-like pattern. Such patterns, called fingerprints, are believed to have two important properties: persistence and uniqueness. Persistence means that fingerprints do not change during a person's lifetime unless a serious injury permanently destroys the pattern. Uniqueness means that fingerprints are so distinctive that each fingerprint is distinct from all other fingerprints. These two properties assure that fingerprints can be used to uniquely establish a person's identity. Fingerprints also have an additional useful property that once a finger touches the surface of an object, an impression, called latent print, is usually left on the surface. The latent fingerprints serve as crucial evidence in criminal investigations and conviction of suspects. These properties make fingerprint an ideal mark of identity for person recognition not only in forensics but also in many government and civilian applications.

The first systematic use of fingerprint recognition began in the early twentieth century [1], as a tool by law enforcement agencies for recognizing repeated offenders and suspects. With advances in automatic fingerprint recognition technology and rapidly growing need for reliable person recognition in our society, fingerprint recognition has found wide adoption in a variety of applications ranging from border control, national ID card, time and attendance, to computer login [2].

Although automatic fingerprint recognition technology has evolved rapidly over the past forty years, a fundamental problem, namely, the probability of observing a particular fingerprint pattern (from amongst billions of such possible patterns), has not been adequately addressed. Our objective is to construct a statistical model for the distribution of fingerprints. Given this model, one can simulate fingerprints and evaluate the probability of observing a specific fingerprint pattern. Statistical modeling of fingerprints is of fundamental importance to a number of problems in fingerprint recognition, including

- Are the minutiae extracted by an algorithm genuine or spurious [3]?
- Has a fingerprint pattern been altered in any way [4]?
- How rare is a latent fingerprint [5]?
- How can we synthesize a large number of different yet realistic fingerprints [6]?
- How should the matching score between two fingerprints be computed [7]?

- How secure is a minutiae template protection technique [8], [9]?

The goal of statistical modeling of fingerprints is to find an explicit expression to approximate the true distribution of fingerprints $f_{\mathbf{I}}(I)$, where I denotes a fingerprint image. Since it is not feasible to directly study the distribution of the grayscale representation of a fingerprint image I due to its high dimensionality[1], we choose to study the distribution of minutiae patterns associated with fingerprints considering the following facts:

- Compact representation. The minutiae template of a slap fingerprint can be stored in about 100 bytes[2], much smaller than the size of the grayscale image.
- Sufficient representation. It has been shown that fingerprint images reconstructed from minutiae can be successfully matched to the original fingerprint [10]–[12].
- High discriminating ability. State of the art fingerprint matchers that are solely based on minutiae have been shown to provide high matching accuracy in several tests conducted by the NIST.
- Wide adoption. Minutiae template is the most widely used representation scheme in automatic fingerprint recognition systems. In addition, human fingerprint examiners perform fingerprint comparison mainly by comparing minutiae; decisions based on minutiae are accepted as evidence in courts of law.

Statistical modeling of minutiae patterns has been studied mainly for estimating fingerprint individuality [5], [13]–[15]. However, most studies (reviewed in [5]) on fingerprint individuality do not derive an explicit model of minutiae patterns which is necessary for an objective assessment. Even when an explicit model is proposed [13]–[15], it is not carefully validated. Furthermore, although statistical minutiae models have potential value in many applications, we have not yet seen any application other than fingerprint individuality assessment.

In this paper a two-level generative model is proposed to approximate the distribution of fingerprint minutiae patterns. The first level of the model approximates the distribution of orientation fields of the fingerprints; the second level utilizes a marked inhomogeneous Poisson point process to model the distribution of minutiae location and polarity. As a second contribution,

[1]The dimensionality of a fingerprint image is defined as the total number of pixels in it. For a 512×480 fingerprint image (such as the fingerprints in NIST SD4), the dimensionality is as high as 245,760.

[2]Under the assumption that each of the three attributes (x, y, α) of a minutia is represented by one byte and a plain fingerprint contains around 30 minutiae.

we propose a minutiae-based fingerprint reconstruction algorithm and apply it to evaluate the proposed minutiae model and two other published minutiae models [13], [15]. Experimental results show that fingerprints reconstructed from minutiae simulated by the proposed model are much more realistic than those from the minutiae simulated by the other two models. As the third contribution, we applied the proposed model to address two specific problems in fingerprint that are of significant interest: (i) recognizing invalid fingerprint minutiae patterns and (ii) incorporating minutiae distinctiveness into match score computation.

The rest of this paper is organized as follows. In section II, the representation of fingerprints is introduced. Section III is devoted to the statistical modeling of minutiae patterns. In section IV, we present the methodology and results of testing minutiae models. Applications of the statistical model are presented in section V. In the final section, we conclude the paper and suggest future research directions.

II. Representation Models

Since the grayscale representation of a fingerprint is not convenient for matching, feature based representations are typically adopted in most fingerprint matching algorithms. In this section, we describe the representation models of fingerprint features including orientation field, singularities, ridge pattern, and minutiae.

A. Modeling Fingerprint Image

Features in fingerprints are generally categorized into three levels (Fig. 1):

1) Level 1 features mainly refer to ridge orientation field and features derived from it, i.e. singularity and pattern type.
2) Level 2 features refer to ridge skeleton and features derived from it, i.e. minutiae.
3) Level 3 features include ridge contours, position and shape of sweat pores and incipient ridges.

Larkin and Fletcher [16] proposed to represent a fingerprint image as a 2D amplitude and frequency modulated (AM-FM) signal:

$$I(x,y) = a(x,y) + b(x,y)\cos(\Psi(x,y)) + n(x,y), \tag{1}$$

which is composed of four components: intensity offset $a(x,y)$, amplitude $b(x,y)$, phase $\Psi(x,y)$, and noise $n(x,y)$. Here we are only interested in the phase $\Psi(x,y)$, since ridges and minutiae

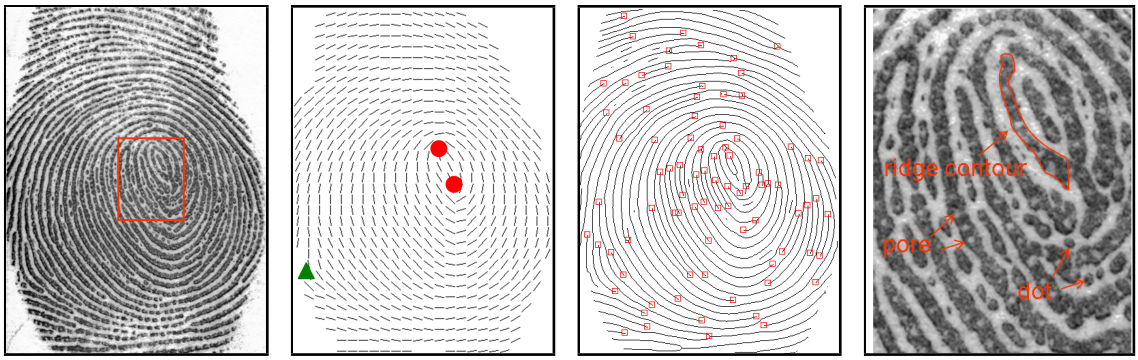

(a) (b) (c) (d)

Fig. 1. Fingerprint features at three levels. (a) Grayscale image (NIST SD30, A067_11), (b) Level 1 features (orientation field, core (red disk), and delta (green triangle)), (c) Level 2 features (ridge skeleton and minutiae), and (d) Level 3 features (ridge contour, pore, and dot) shown only for the subimage marked in (a).

are completely determined by the phase provided we do not consider Level 3 features (such as sweat pores and ridge contour). Therefore, a fingerprint can be approximated by a 2D FM signal:

$$I(x, y) = \cos(\Psi(x, y)). \tag{2}$$

The gradient of the phase $\Psi(x, y)$ is also termed as instantaneous frequency. In a fingerprint image, the direction of instantaneous frequency is normal to the local ridge orientation and the magnitude of instantaneous frequency determines the local ridge frequency.

B. Modeling Orientation Field

The orientation field of a fingerprint can be represented as the sum of a continuous orientation field and a singular orientation field [17]–[19].

$$\Theta(x, y) = \Theta_C(x, y) + \Theta_S(x, y). \tag{3}$$

Hereinafter, $\Theta(x, y)$ is also termed as the composite orientation field to reflect the fact that it consists of the continuous orientation field $\Theta_C(x, y)$ and the singular orientation field $\Theta_S(x, y)$.

The singular orientation field is defined by the singular points (core and delta) in a fingerprint [17]:

$$\Theta_S(m, n) = \frac{1}{2} \sum_{i}^{M} t_i \arctan(\frac{y - y_i}{x - x_i}), \tag{4}$$

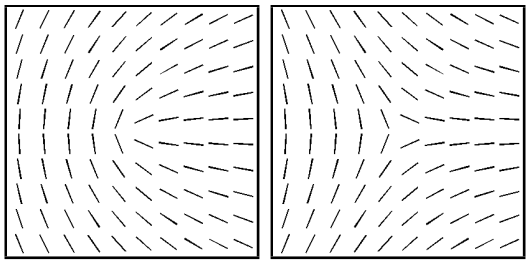

(a) (b)

Fig. 2. Orientation field of (a) core type singularity and (b) delta type singularity. The singular points are located in the image center.

where M denotes the number of singular points, (x_i, y_i) denotes the coordinate of the ith singularity, and $t_i \in \{1, -1\}$ denotes its type (core: 1, delta: -1). Figure 2 shows the orientation fields of a core type and a delta type singularity.

The continuous orientation field does not contain any singularity and looks like the orientation field of a plain arch type fingerprint. To decompose an orientation field, we first detect singular points using the Poincaré index method [2] and then use equations (3) and (4) to obtain $\Theta_S(x, y)$ and $\Theta_C(x, y)$. Figure 3 shows the decomposition of the orientation field of a fingerprint.

C. Modeling Ridge Pattern

In the FM model, ridge pattern is determined by the phase. According to the Helmholtz Decomposition Theorem [20], the phase can be represented as the sum of continuous phase and spiral phase:

$$\Psi(x, y) = \Psi_C(x, y) + \Psi_S(x, y). \tag{5}$$

Hereinafter, the phase $\Psi(x, y)$ is also termed as the composite phase to reflect the fact that it consists of the continuous phase $\Psi_C(x, y)$ and the spiral phase $\Psi_S(x, y)$.

The spiral phase $\Psi_S(x, y)$ consists of a set of N spirals, each of which corresponds to a minutia:

$$\Psi_S(x, y) = \sum_{i=1}^{N} p_i \arctan(\frac{y - y_i}{x - x_i}), \tag{6}$$

where (x_i, y_i) denotes the coordinate of the ith minutia and $p_i \in \{1, -1\}$ denotes its polarity. The similarity between equations (4) and (6) indicates that minutia can be deemed as a kind of singularity in the phase image. When the direction of a minutia (shown in Fig. 4) is the same

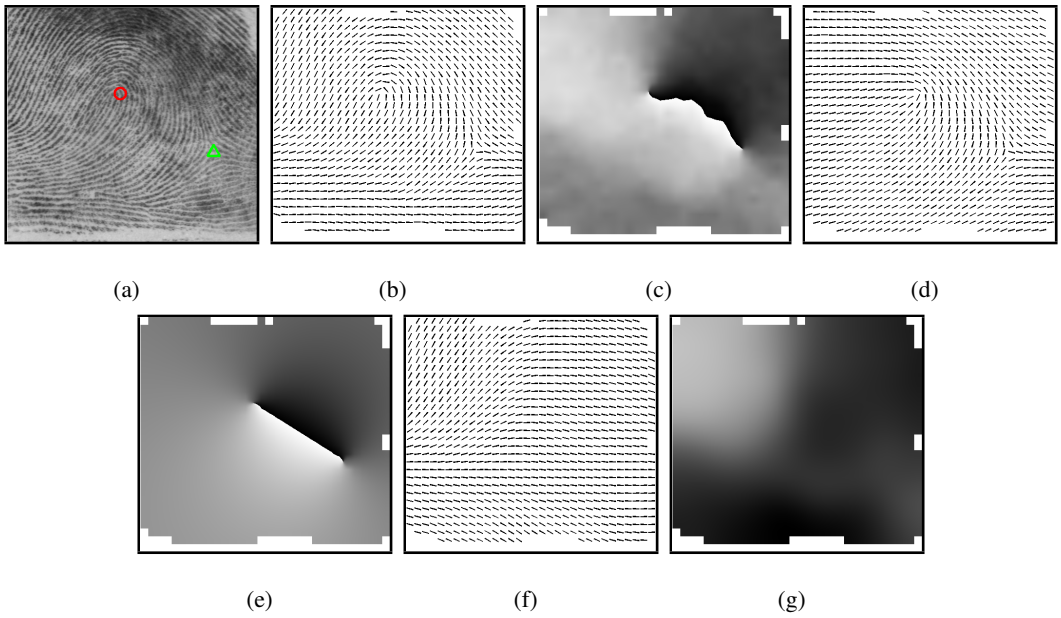

Fig. 3. Decomposition of an orientation field. (a) A fingerprint image with singular points overlaid (◯ denotes core and Δ denotes delta), (b) composite orientation field, (c) composite orientation field shown as a grayscale image, (d) singular orientation field, (e) singular orientation field shown as a grayscale image, (f) continuous orientation field, and (g) continuous orientation field shown as a grayscale image.

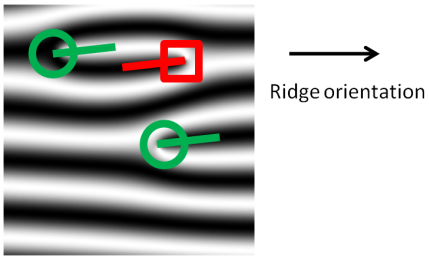

Fig. 4. The polarity of a minutia is defined based on its direction and local ridge orientation. The polarity of the two minutiae marked by ◯ is positive and the polarity of the minutia marked by □ is negative. Along the local ridge orientation (shown as an arrow), a positive minutia introduces a ridge and a negative minutia consumes a ridge.

as the local ridge orientation, the polarity of the minutia is positive $(+1)$ and the minutia is referred to as a positive minutia. On the other hand, when the minutia direction is opposite to the local ridge orientation, its polarity is negative (-1) and the minutia is referred to as a negative minutia. In other words, given the orientation field, the direction of a minutia is determined by its polarity.

The continuous phase $\Psi_C(x, y)$ does not contain any spiral. To decompose the composite

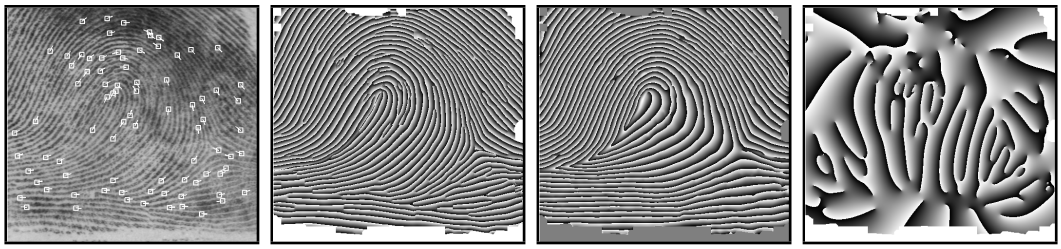

(a) (b) (c) (d)

Fig. 5. Decomposition of fingerprint phase. (a) A fingerprint image with minutiae overlaid, (b) composite phase, (c) continuous phase, and (d) spiral phase.

phase, we first detect spirals using the algorithm in [21] and then use equations (5) and (6) to obtain $\Psi_S(x, y)$ and $\Psi_C(x, y)$. Figure 5 shows the decomposition of the phase of a fingerprint.

III. Statistical Models

In this section, we first discuss the motivation of modeling fingerprint minutiae as a two-level generative model and then describe each level of the model respectively.

A. Modeling Fingerprint Image

A statistical model of fingerprints attempts to find an explicit expression to approximate the true distribution of fingerprints, $f_{\mathbf{I}}(I)$, where I denotes a fingerprint image. Since it is not feasible to directly study the distribution of the grayscale representation of a fingerprint I due to its high dimensionality, we choose to study the distribution of fingerprint features. Several recent studies have shown that Level 3 features only have a secondary role in discriminating fingerprints [22], [23]. For this reason, we assume that a fingerprint image I is represented by its orientation field Θ and minutiae set $\mathbf{x}$. The probability distribution of a fingerprint I can be approximated by the joint density of its orientation field Θ and minutiae pattern $\mathbf{x}$.

$$f_{\mathbf{I}}(I) = f_{\mathbf{X\Theta}}(\mathbf{x}, \Theta). \tag{7}$$

Kücken and Newell [24] argue that fingerprint is the result of a buckling process in the basal cell layer of the fetal epidermis; the stresses causing the buckling process come from the finger creases, nail furrows, and volar pads. The well-known fingerprint synthesis software, SFinGe [6], first synthesizes an orientation field and then performs iterative Gabor filtering on a randomly

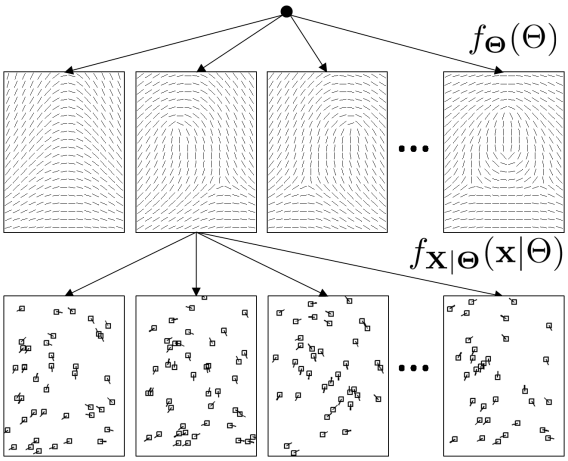

Fig. 6. Two-level statistical model of minutiae patterns.

seeded image to generate a fingerprint. Both the fingerprint formation theory [24] and the two-stage fingerprint synthesis procedure [6] suggest that we should first model the orientation field, Θ, and then model the minutiae pattern, $\mathbf{x}$, conditioned on the orientation field (see Fig. 6).

$$f_{\mathbf{X}\mathbf{\Theta}}(\mathbf{x}, \Theta) = f_{\mathbf{\Theta}}(\Theta) f_{\mathbf{X}|\mathbf{\Theta}}(\mathbf{x}|\Theta), \tag{8}$$

where $f_{\mathbf{X}|\mathbf{\Theta}}(\mathbf{x}|\Theta)$ denotes the probability of a minutiae pattern given the orientation field. According to fingerprint formation theory [24], the same orientation field can correspond to a number of different minutiae patterns. This phenomenon has been observed in fingerprint synthesis experiments [6] as well as in the fingerprints of identical twins [25]. As an example, different minutiae patterns with the same orientation field are shown in Fig. 7.

In the following subsections, we describe the two levels of the fingerprint model: orientation field model and minutiae pattern model.

B. Modeling Orientation Field

An orientation field is represented as the sum of singular orientation field and continuous orientation field, as described in Section II-B. However, both the singularity features (type and location) and the continuous orientation field are not fixed-length feature vectors which makes the statistical modeling problem challenging. To convert an orientation field to a fixed-length

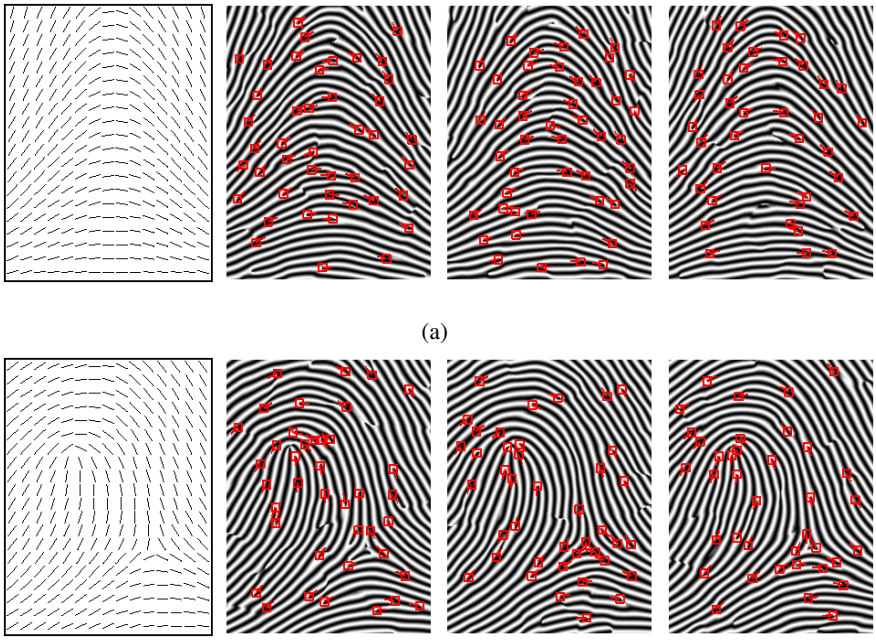

(a)

(b)

Fig. 7. Different fingerprints (minutiae patterns) with the same orientation field: (a) arch-type orientation field followed by three arch-type images with different minutiae patterns and (b) left loop-type orientation field followed by three left loop-type images with different minutiae patterns.

feature vector, we treat three major types of fingerprints (arch, loop, and whorl) separately[3], and model the continuous orientation field by polynomials. As a result, the singularity features and polynomial coefficients constitute a fixed-length feature vector, which is termed as the orientation vector. While the probability distribution of fingerprint singularities has been studied by Cappelli and Maltoni [27], we consider the probability distribution of the whole orientation field here. Another difference from the model in [27] is that we study the distribution of singularities in fingerprints of left loop, right loop, and tented arch together, since (i) all these three classes contain one core and one delta and (ii) there are no absolute separating lines between these three classes.

Let $\mathbf{s} = (x_1, y_1, \cdots, x_t, y_t)$ be the set of singularity features of a fingerprint, where t denotes the number of pairs of cores and deltas in the fingerprint. Note that $t = 0, 1, 2$ for arch, loop,

[3]According to the statistics reported in the document of the NIST SD14 database [26], around 99.7% of all fingerprints belong to these three major types (arch: 3.6%, loop: 68.3%, and whorl: 27.8%).

and whorl type, respectively. The sine and cosine of the doubled continuous orientation field[4] are modeled by two polynomials of order m, respectively:

$$\sin(2\Theta(x,y)) = f_{sin}(m,\mathbf{a};x,y) = \sum_{i+j\leq m} a_{ij}x^i y^j, \tag{9}$$

and

$$\cos(2\Theta(x,y)) = f_{cos}(m,\mathbf{b};x,y) = \sum_{i+j\leq m} b_{ij}x^i y^j. \tag{10}$$

The orientation vector is obtained by combining three feature vectors:

$$\mathbf{A} = \begin{pmatrix} \mathbf{s} \\ \mathbf{a} \\ \mathbf{b} \end{pmatrix}. \tag{11}$$

The probability density of orientation field is given by

$$f_{\mathbf{\Theta}}(\Theta) = \sum_{t=0,1,2} w_t p_t(\mathbf{A}), \tag{12}$$

where w_t denotes the a priori probability of fingerprints with t pairs of cores and deltas, and $p_t(\mathbf{A})$ represents the probability density of orientation vectors of fingerprints of type t. The density $p_t(\mathbf{A})$ is approximated by a Gaussian mixture model:

$$p_t(\mathbf{A}) = \sum_{k=1}^{K_t} \pi_{tk}\mathcal{N}(\mathbf{A}|\mu_{tk},\mathbf{\Sigma}_{tk}), \tag{13}$$

where K_t denotes the number of Gaussians, π_{tk} denotes the kth mixing probability, and $\mathcal{N}(\cdot)$ denotes the Gaussian PDF.

C. Modeling Minutiae Pattern

A minutiae pattern is a set of marked points in two-dimensional space, $\mathbf{x} = \{(x_1,p_1),\cdots,(x_n,p_n)\}$, where x_i is the location of a minutia, and its mark is its polarity $p_i \in \{+1,-1\}$. Notice that in contrast to the traditional definition of minutiae [2], this definition does not contain minutiae direction since the direction is fully determined by the polarity and orientation field. Decoupling minutiae from orientation field enables modeling minutiae patterns using relatively simple models.

[4]The orientation value is doubled in order to avoid discontinuity between θ and $\theta+\pi$.

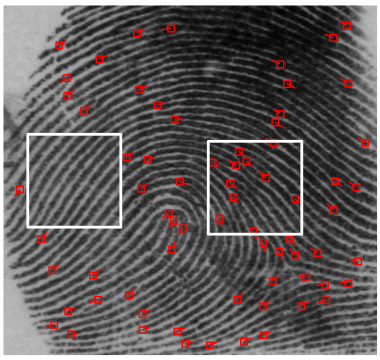

Fig. 8. The left box contains no minutia, while the right one contains eleven minutiae. This image is from NIST SD4, F0017.

A minutiae pattern $\mathbf{x}$ can be deemed as a realization of a spatial point process $\mathbf{X}$ [28]. A spatial point process is a random set of points, in which both the number of points and the location of the points are random. To determine an appropriate point process model for minutiae patterns, let us first consider only the location of minutiae. The homogeneous Poisson point process [28] is the most basic model of a point process. A homogeneous Poisson point process with density $\lambda > 0$ has the following properties:

1) The number of points falling in any region A follows a Poisson distribution with mean $\lambda \cdot area(A)$. The probability mass function of a Poisson distribution with mean λ is:
$$f_{Poisson}(n;\lambda) = \frac{\lambda^n}{n!}e^{-\lambda}. \tag{14}$$
2) Given that there are n points inside a region A, the locations of these points are i.i.d. with uniform distribution inside A.
3) The sets of points in two disjoint regions A and B are independent. Both the number and the location of the points in the two sets are independent.

The homogeneous Poisson point process is not suitable for minutiae patterns, since the distribution of minutiae in fingerprints is apparently not uniform. There are generally an excess number of minutiae in the area where the ridges either converge or diverge, for example around the singular points. Figure 8 illustrates this fact. To account for the nonuniformity of minutiae, the first two properties of the homogeneous Poisson point process should be modified as follows:

1) The number of points falling in any region A follows a Poisson distribution with mean $\int_A \lambda(u)du$, where $\lambda(u), u \in \mathbb{R}^2$ represents the density of points at u;

2) Given that there are n points inside a region A, the locations of these points are i.i.d. and further, they are distributed with probability density $f(u) = \lambda(u)/\Lambda(A)$, where $\Lambda(A) = \int_A \lambda(u)du$.

This results in an inhomogeneous Poisson point process with density function $\lambda(u)$. Given that there are n points inside a region A, the density of the locations of these points is given by

$$f_n(\mathbf{x}) = \prod_{i=1}^{n} \frac{\lambda(x_i)}{\Lambda(A)}. \tag{15}$$

Next we consider the polarity of minutiae. Using the arch-type fingerprints in Fig. 7(a) as an example, where the ridges are flowing from left to right, ridges first diverge producing many positive minutiae, and then converge producing many negative minutiae. This indicates that minutiae with the same polarity tend to form clusters. Thus we use two different inhomogeneous Poisson point processes to model positive and negative minutiae.

In summary, a minutiae pattern $\mathbf{x}$ is viewed as a union of two subsets of minutiae, a positive minutiae pattern $\mathbf{x}_p$ containing all positive minutiae in $\mathbf{x}$, and a negative minutiae pattern $\mathbf{x}_n$ containing all negative minutiae in $\mathbf{x}$. As a result, the minutiae pattern $\mathbf{x}$ is viewed as a realization of two independent inhomogeneous Poisson point processes $\mathbf{X}_p$ and $\mathbf{X}_n$ with density functions $\lambda_p(u)$ and $\lambda_n(u)$, respectively.

D. Parameter Estimation

The a priori probabilities of three major types of fingerprints are reported in the document of the NIST SD14 database [26]. The parameters of the mixture model of orientation field in Equation (13) are estimated using orientation vectors of fingerprints in the NIST SD4 database. For reliable parameter estimation, the singular points of all these fingerprints are manually marked and only those fingerprints (a total of 1,215) with complete singularity information are used.

The inhomogeneous Poisson point process model of minutiae patterns is fully determined by its density function $\lambda(u)$. To estimate the minutia density of a given orientation field, we need a training set of minutiae patterns with the same orientation field. Due to the difficulty of finding many true fingerprints with the same orientation field, we used a number of synthesized fingerprints. Based on the given orientation field and a fixed ridge frequency (0.1 ridges per

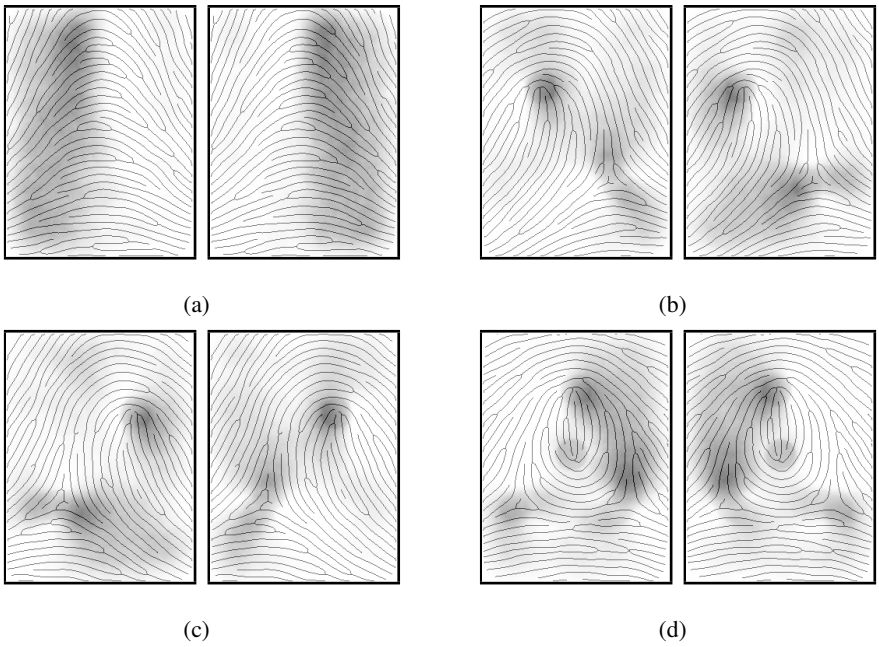

Fig. 9. Density maps of positive and negative minutiae in fingerprints of different pattern types: (a) arch, (b) left loop, (c) right loop, and (d) whorl. Dark pixels indicate higher minutiae density. Ridge skeleton of an example fingerprint of corresponding pattern type is overlaid on the density maps for illustration purpose.

pixel), a set of 100^5 synthetic fingerprint images (with the same orientation field) are generated by performing iterative Gabor filtering on random seed images. Minutiae are then detected in these fingerprints and classified as positive or negative. Parzon window method is used to separately estimate the density of positive and negative minutiae at each location in the fingerprint. Gaussian kernel with a standard deviation of 20 pixels is used as the window function.

The two minutiae density maps[6] for the arch-type fingerprint in Fig. 7(a) are shown in Fig. 9(a). We can observe that (i) positive minutiae dominate the left side and negative minutiae dominate the right side of the arch-type fingerprint, (ii) minutiae density is higher in the top portion of the image due to the convergence and divergence of orientation field, and (iii) due to the symmetry of arch-type orientation field, the density maps of positive and negative minutiae are quite symmetric. The two minutiae density maps for the left loop-type fingerprints in Fig. 7(b)

[5]We found in the experiment that the estimates obtained using 100 fingerprints are very similar to the estimates using 200 or more fingerprints.

[6]Note that minutiae density maps shown in previous studies, such as [10], do not consider positive and negative minutiae separately.

are shown in Fig. 9(b). These two density maps appear very different from the density maps of arch-type fingerprints, indicating that decoupling minutiae from orientation field is necessary to simplify the minutiae modeling problem. But we do observe a common phenomenon in both types of fingerprints, namely, the density maps of positive and negative minutiae are complementary to each other. In other words, at each location in the fingerprint the dominating polarity is either positive or negative and only at a few locations, the densities of minutiae with the two polarities are balanced. A similar analysis can also be done for the density maps of right loop-type and whorl-type fingerprints (see Fig. 9).

IV. Validation

A statistical model of fingerprint minutiae should be able to simulate a set of synthetic minutiae patterns which are realistic as well as have statistics similar to true fingerprint minutiae. In this section, we first describe the minutiae simulation algorithm of the proposed minutiae model. Then we present a new minutiae based fingerprint reconstruction algorithm which is used to validate whether the simulated minutiae patterns are realistic. Finally, a statistical test of the minutiae model is discussed.

A. Minutiae Simulation

A minutiae pattern is simulated by first generating an orientation field followed by generating a minutiae pattern conditioned on the orientation field.

1) Orientation Field Generation: An orientation field is generated through the following steps: (i) select a fingerprint pattern type (arch, loop, or whorl) according to the a priori probability of fingerprint patterns, (ii) generate an orientation vector $\mathbf{A}$ according to the Gaussian mixture model in Equation (13), (iii) compute the singular orientation field using Equation (4), (iv) compute the continuous orientation field using Equations (9) and (10), and finally (v) compute the orientation field using Equation (3).

2) Minutiae Pattern Generation: A minutiae pattern is generated by first simulating two inhomogeneous Poisson point processes, one for positive minutiae and the other for negative minutiae, and then combining the two patterns. The flowchart of the minutiae simulation algorithm is given in Fig. 10. The two density maps of the given orientation field are estimated using the approach described in Section III-D. An inhomogeneous Poisson point process is simulated by the rejection

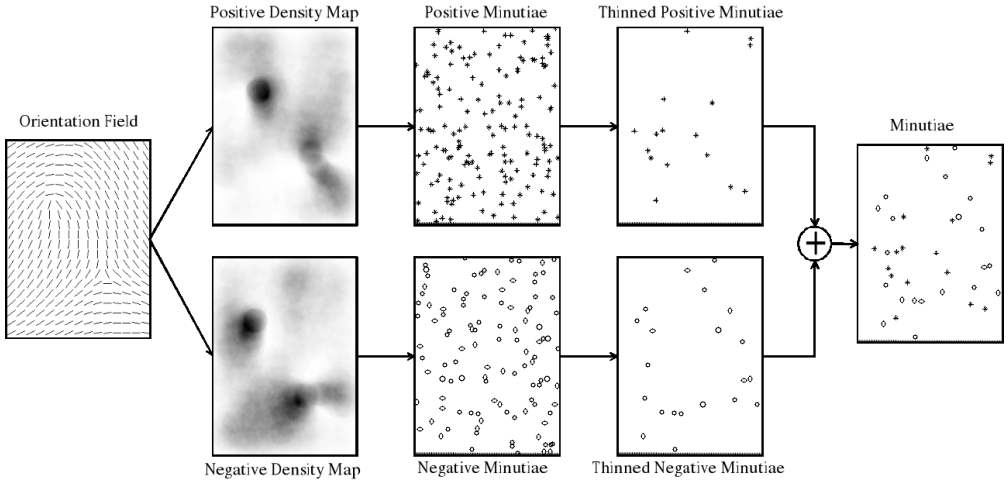

Fig. 10. Flowchart of the minutiae pattern simulation algorithm for a given orientation field.

method [29]. This method consists of two steps. First, a sample of the homogeneous Poisson process with density $\lambda^* = max(\lambda(u))$ is generated. Simulation of an homogeneous Poisson point process consists of two steps as well. The number n of points is first sampled from a Poisson distribution with mean $\lambda^* \cdot area(A)$. Then n points are sampled independently from a uniform distribution over the region A. Due to the use of a large density λ^*, the number n of points simulated in the first step is much higher than in the final pattern. In the second step, an independent, location-dependent thinning procedure is performed. For each point in the sample $\{x_1, \cdots, x_n\}$ simulated, a decision is made as to whether to "retain" or "thin" it. A point x_i is retained with probability $p_{x_i} = \lambda(x_i)/\lambda^*$ and a point is retained or deleted independently of what happens to any of the other points. A set of minutiae patterns simulated using this method is shown in Fig. 11. Note that the direction of a minutia is obtained based on the minutia polarity and local ridge orientation.

B. Visual Validation

Given a set of N fingerprint minutiae $\{x_i, y_i, \alpha_i\}, 1 \leq n \leq N$, where ($x_i$, y_i) and α_i denote the location and direction of the ith minutia, respectively, the goal of fingerprint reconstruction is to reconstruct a fingerprint image with the same minutiae pattern as the given minutiae pattern. Reconstructing a fingerprint that is consistent with the given minutiae pattern is known to be difficult [10], [11]. The line drawing approach [10] is not very successful in reconstructing

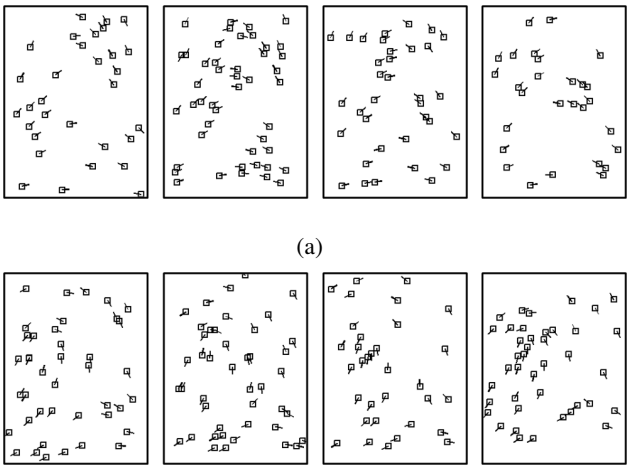

(a)

(b)

Fig. 11. Minutiae patterns simulated according to the proposed model: (a) four minutiae patterns of arch type and (b) four minutiae patterns of left loop type.

a complete and realistic fingerprint. The iterative Gabor filtering approach [11] is known to generate some spurious minutiae and may even annihilate or shift the given minutiae. Based on Frequency Modulation (FM) model and Holmholz phase decomposition theorem [16], Feng and Jain [12] first reconstructed the continuous phase and then combined it with the spiral phase to obtain the reconstructed fingerprint image. Although such an approach can avoid generating spurious minutiae in principle, spurious minutiae are still introduced in practice. The reason for spurious minutiae is that the "continuous" phase reconstructed by the algorithm in [12] is not really continuous.

The goal of the proposed reconstruction algorithm is to reconstruct the FM representation of the original fingerprint, $cos(\Psi(x, y))$. To obtain the phase $\Psi(x, y)$, the following three steps are performed: (i) orientation field reconstruction, (ii) continuous phase reconstruction, and (iii) combination of the spiral phase and the continuous phase. The flow chart of the proposed fingerprint reconstruction algorithm is depicted in Fig. 12. While this reconstruction algorithm uses a similar framework as [12], it differs in how the continuous phase is reconstructed from an orientation field. Piecewise planar model was used to model continuous phase in [12]. In contrast, here we employ a non-parametric approach to construct the continuous phase (see the flowchart in Fig. 13), which is more effective since it can generate fingerprints consistent with the given minutiae patterns.

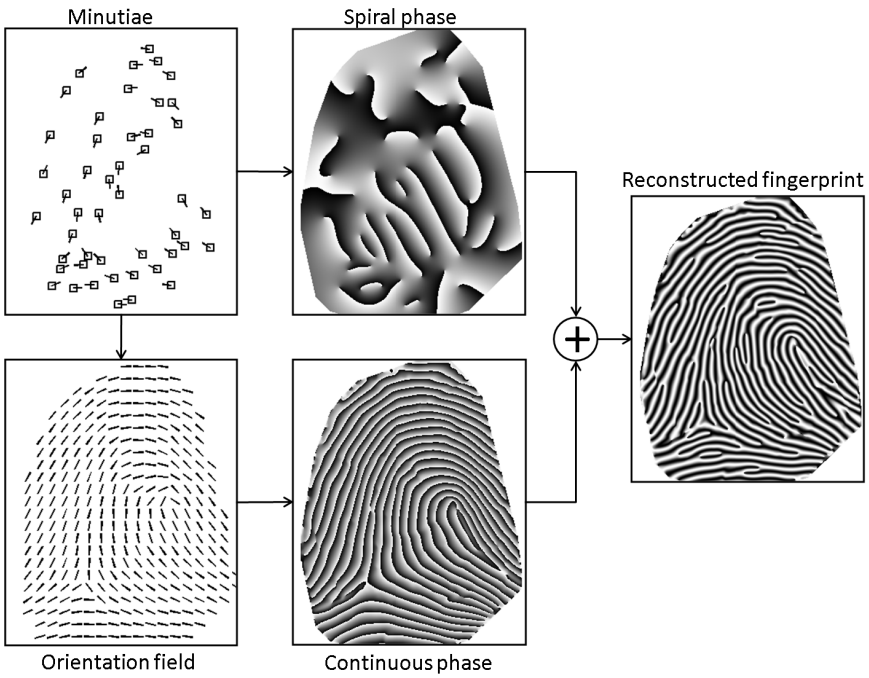

Fig. 12. Flow chart of the proposed fingerprint reconstruction algorithm.

The main steps of the continuous phase reconstruction algorithm are given below:

1) A complex valued fingerprint image $I = I_{real} + i \cdot I_{imag}$ is generated by performing iterative complex Gabor filtering on a seed image initialized by random noise.
2) The composite phase of fingerprint I is given by $\arctan(I_{real}, I_{imag})$.
3) Spirals are detected from the composite phase image using the algorithm in [21] and the spiral phase is computed using equation (6).
4) The continuous phase is obtained by subtracting the spiral phase from the composite phase.

This algorithm can be viewed as first generating a fingerprint using a SFinGe like approach and then extracting the continuous phase of the fingerprint.

A good reconstruction algorithm should preserve almost all of the given minutiae and produce very few spurious minutiae. As we can see from the example in Fig. 14, using the piecewise planar model of [12], eleven of the given minutiae are missed and 10 spurious minutiae are produced. However, using the proposed algorithm, only two of the given minutiae are missed and no spurious minutiae are produced. In addition, the fingerprint reconstructed by the proposed

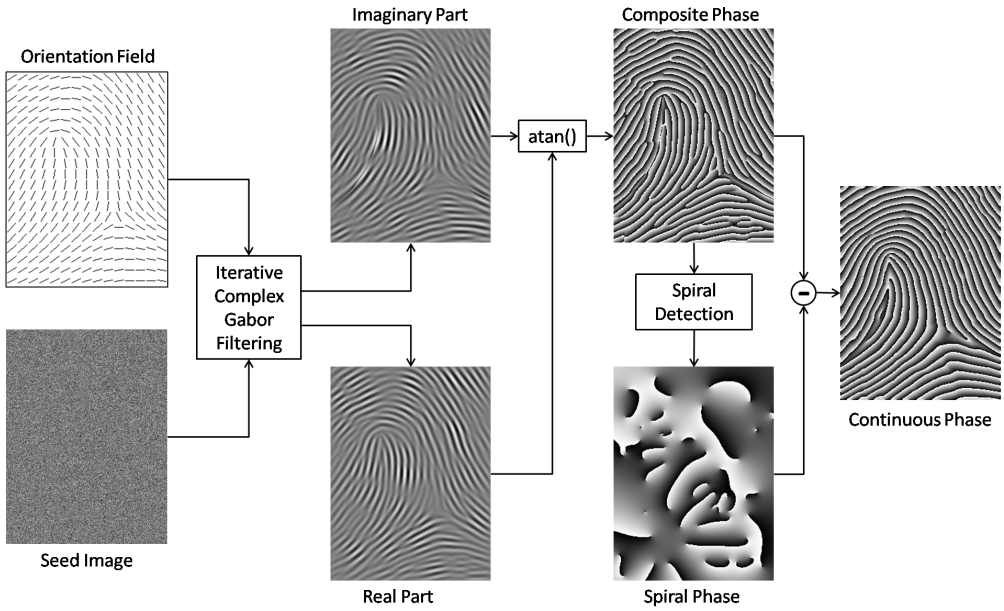

Fig. 13. Constructing the continuous phase from a given orientation field.

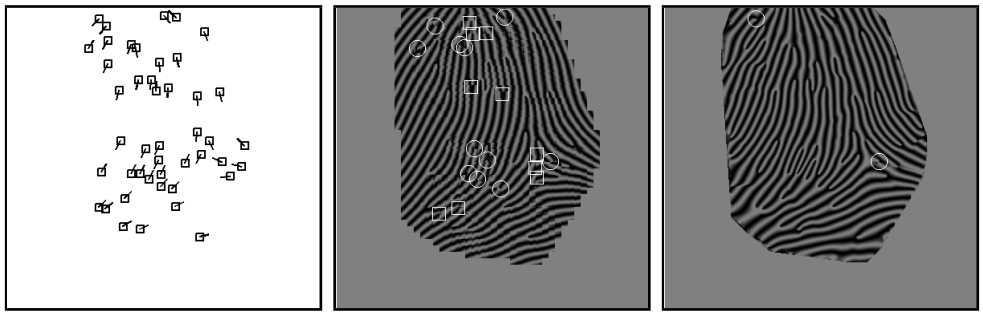

(a) (b) (c)

Fig. 14. Fingerprint reconstruction from a given minutiae pattern: (a) Minutiae pattern, (b) reconstructed fingerprint by the piecewise planar model [12], and (c) reconstructed fingerprint by the proposed algorithm. Missed minutiae are marked by ◯ and spurious minutiae are marked by □.

algorithm is smoother.

To validate a statistical model of minutiae, minutiae patterns are simulated from the model, followed by fingerprint image reconstruction. If the reconstructed image appears unrealistic, we assert that the statistical model is not valid. Note that this validation is based on visual observation and it is a necessary but not sufficient condition for the validity of a minutiae model. A statistical and quantitative test, which will be described in the next section, has to be conducted to validate

the model.

Figure 15(a) shows a set of minutiae patterns simulated using the uniform distribution model of Pankanti et al. [13], where both the position and direction of a minutia are modeled by independent uniform distributions. While it is difficult to determine whether this minutiae distribution model is valid by observing the synthesized minutiae patterns, we can easily glean that the uniform distribution model is not appropriate by observing the reconstructed fingerprint images. Figure 15(b) shows a set of minutiae patterns simulated using the mixture model of Chen and Jain [15]. In the mixture model [15], minutiae in fingerprints of the same pattern type are clustered into several clusters. In each cluster, the minutia position is modeled by a bivariate Gaussian distribution, the minutia direction is modeled by von Mises distribution, and the position and the direction of a minutia are assumed to be conditionally independent of each other. Again, by observing the fingerprint images reconstructed from the simulated minutiae patterns, we conclude that the mixture model is not valid. Compared with the reconstructed images of these two minutiae models, the images (shown in Fig. 15(c)) reconstructed from the minutiae simulated by the proposed minutiae model are much more realistic.

C. Statistical Test

We have conducted a formal goodness-of-fit test for the proposed minutiae model. The envelope test introduced by Ripley [30] is used. The idea is to compare the empirical summary characteristic estimated from true minutiae patterns to estimates of the summary characteristic for simulated minutiae pattern. The summary characteristic used is the nearest neighbor distribution function, $D(r)$, which represents the probability that the distance between a minutia and its nearest neighbor is less than r. The estimate of $D(r)$, $\hat{D}(r)$, is obtained from a sample of 100 different fingerprints (with the same orientation field) simulated by performing iterative Gabor filtering on random seed images. A total of $k = 100$ minutiae patterns are simulated using the proposed model. For each simulated minutiae pattern, the estimate $\hat{D}_i(r)$ for $i = 1, \cdots, k$, is determined. The extreme values

$$D_{min}(r) = \min_{(i)} \hat{D}_i(r) \tag{16}$$

$$D_{max}(r) = \max_{(i)} \hat{D}_i(r) \tag{17}$$

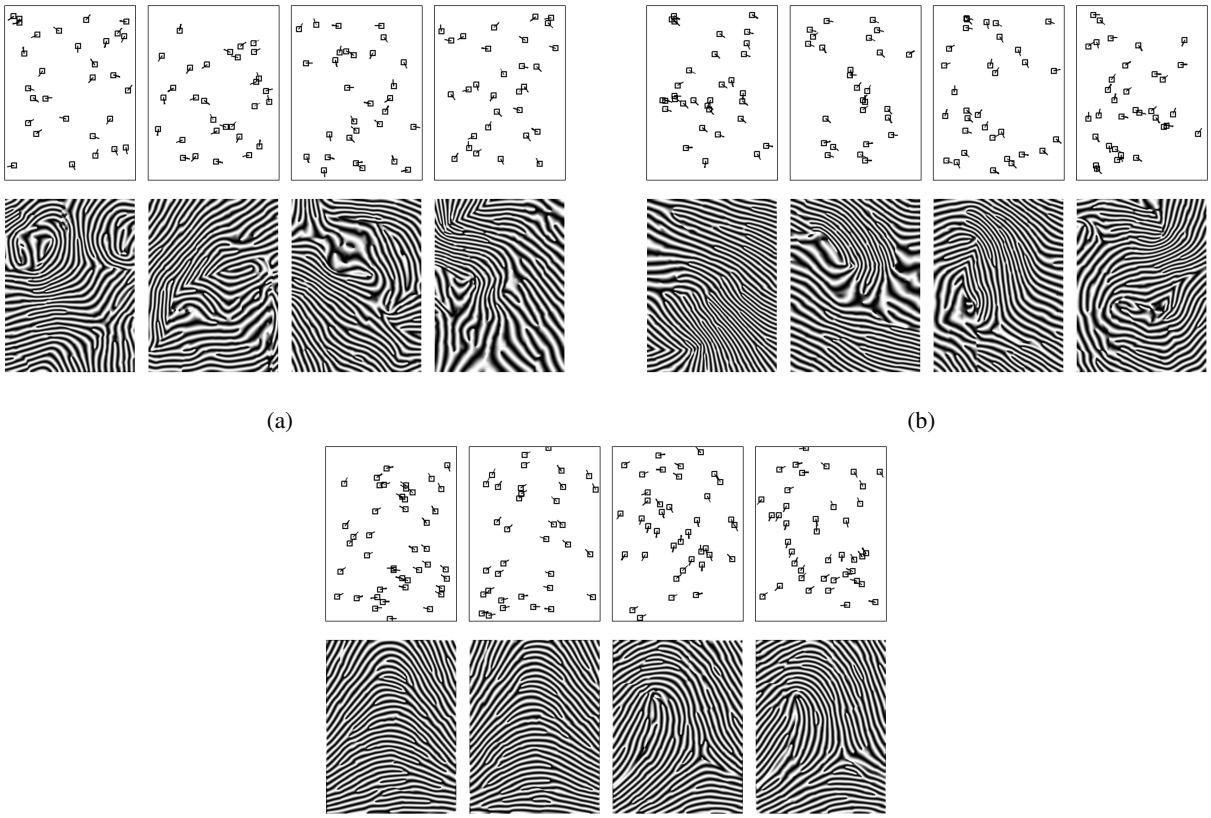

Fig. 15. Minutiae patterns simulated by three different minutiae distribution models and the reconstructed fingerprint images from these minutiae patterns. (a) Uniform model of [13], (b) mixture model of [15], and (c) proposed model.

are obtained. If the inequality

$$D_{min}(r) \leq \hat{D}(r) \leq D_{max}(r) \tag{18}$$

holds for all r, namely the empirical summary characteristic is enclosed by the envelope, the model is accepted, otherwise it is rejected. We conducted this test for models of four types of fingerprints (namely, arch, left loop, right loop, and whorl) in Fig. 9. As shown in Fig. 16, the inequality holds for all r in all cases and thus the proposed marked inhomogeneous Poisson point process model is accepted and is valid.

V. Applications

A statistical model of fingerprint minutiae can be used for several applications dealing with fingerprint analysis. In this section, we present two applications of the proposed model: (i)

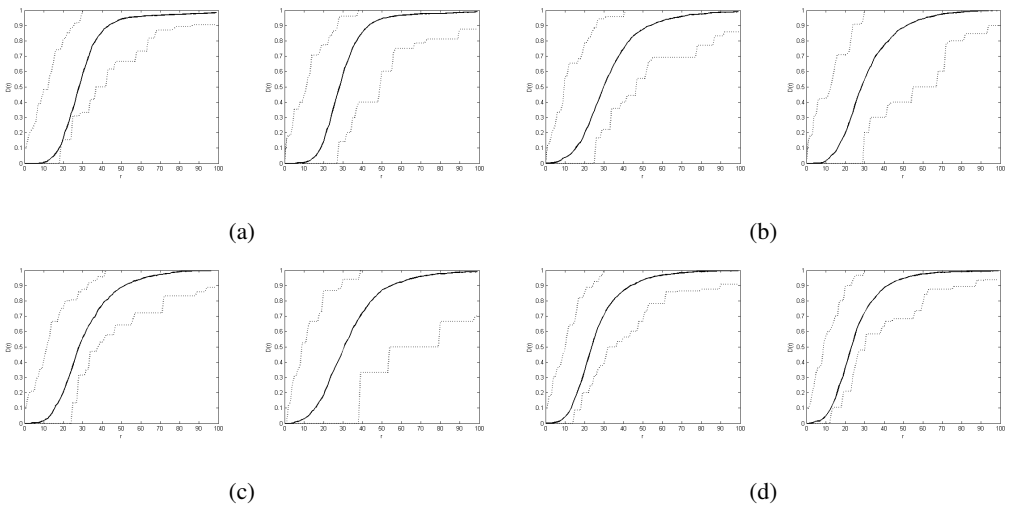

Fig. 16. Envelope test of positive and negative minutiae models in fingerprints of four different pattern types: (a) arch, (b) left loop, (c) right loop, and (d) whorl. Solid lines represent the distribution of nearest neighbor distances based on synthetic fingerprint images and dotted lines are the envelopes.

determining whether a minutiae pattern comes from a valid fingerprint and (ii) use distinctiveness of minutiae to improve match score computation.

A. Recognizing Non-Fingerprint Patterns

Given a set of minutiae (with direction), can we tell if it is a valid fingerprint minutiae pattern or not? In other words, we would like to know if the given set of minutiae were indeed extracted from a fingerprint image. Invalid fingerprint images or minutiae patterns may be encountered due to various reasons. In multibiometrics databases maintained by law enforcement agencies, other biometric traits, such as face or iris, may be incorrectly labeled as fingerprints due to some mistakes; Minutiae templates in crucial databases may be purposely modified by attackers. It is desired to have a validation algorithm to detect such invalid fingerprint patterns in order to maintain the integrity of large scale fingerprint databases.

The proposed validation algorithm consists of two steps: (i) orientation field validation and (ii) minutiae validation. The orientation field validation algorithm determines whether the orientation field reconstructed from the given minutiae pattern is valid. If the orientation field is not valid, the minutiae pattern is deemed as not valid. Otherwise, the minutiae validation algorithm checks whether the distribution of the minutiae is valid.

To validate if a minutiae pattern comes from a valid orientation field, the orientation field is reconstructed from the given minutiae pattern using the algorithm in [12]. Fourth order polynomials are fitted to the reconstructed orientation field and the orientation field is represented by the coefficients of the polynomials[7]. The vector of coefficients is termed as orientation vector and contains 30 coefficients. The distribution of polynomial coefficients is modeled by a Gaussian mixture model (see Equation (13)), whose parameters are estimated using 1,125 good quality fingerprints (with NFIQ [31] value of 1 or 2) in the NIST SD4 database. Given a reconstructed orientation field, the probability density of its orientation vector is evaluated using Equation (13). The logarithm of probability density is linearly mapped to a number in the range $[0, 1]$, which is termed as validity score.

To validate the distribution of a minutiae pattern which passes the orientation field validation, we compare the two density maps (positive and negative) of the given minutiae pattern with the corresponding density maps of simulated fingerprints with the same orientation field. Specifically, the mean of the absolute difference between corresponding density maps is computed. The negative of the mean is linearly mapped to a validity score in the range $[0, 1]$. The assumptions made here are: (i) synthetic fingerprints simulated using an iterative contextual filtering algorithm [6] are valid, and (ii) the density maps of a valid minutiae pattern should be similar to the density maps of these synthetic fingerprints with the same orientation field.

To evaluate the proposed orientation field validation algorithm, we collected true minutiae patterns from 100 fingerprints in NIST SD4 (not included in the training set) and three types of invalid minutiae patterns: (i) minutiae extracted from 100 face images in the FERET database [32], (ii) minutiae extracted from 100 iris images in the CASIA-IrisV3 database [33], and (iii) 100 synthetic minutiae patterns simulated using the uniform model [13]. Minutiae in all fingerprint, face, and iris images are extracted using the same fingerprint feature extraction algorithm in Neurotechnology VeriFinger 6.2 SDK [34]. Figure 17 shows the distributions of the validity scores of these four types of minutiae patterns. As shown in Fig. 17, the distributions of the three types of invalid minutiae patterns are well separated from the distribution of true minutiae patterns. The examples in Fig. 18 clearly show that the reconstructed orientation fields from

[7]To avoid the difficulty in modeling caused by missing or spurious singular points in true fingerprint images, the polynomial model is directly used to approximate the composite orientation field.

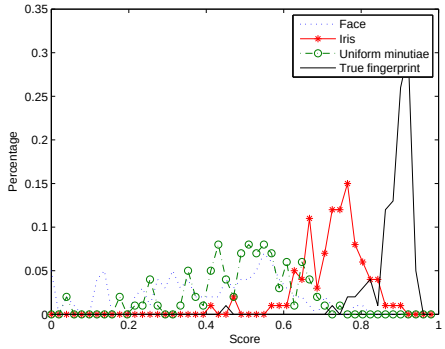

Fig. 17. Distributions of validity scores at the orientation field level for minutiae patterns extracted from face images, iris images and true fingerprint images, and synthetic minutiae patterns simulated by the uniform model [13].

three types of invalid minutiae patterns are not valid. Figures 17 and 18 also indicate that the reconstructed orientation field of iris is closer to true fingerprint orientation field than face or minutiae simulated by the uniform model.

To evaluate the proposed minutiae pattern validation algorithm, we generate minutiae (with location and polarity) using the uniform model while the direction of each minutia is taken from true orientation field. This can be viewed as an improved uniform model. The true minutiae patterns used are the same as in the first experiment (from NIST SD4). Figure 19 shows the distributions of the validity score of simulated minutiae patterns and true minutiae patterns. The two distributions are also well separated, even though the simulated minutiae patterns using the improved uniform model appear quite natural to human eye, as shown in Fig. 20. However, when the true minutiae pattern contains a large number of spurious minutiae as shown in Fig. 20(c), its validity score might be lower than the validity scores of some simulated minutiae patterns using the improved uniform model.

B. Minutia Distinctiveness

The number of matched minutiae pairs is an important factor in computing the match score between two fingerprints [35], [36]. However, typically all the matched minutiae pairs are treated equally.

For a minutia p in fingerprint A, the probability that it has a matched minutia q in fingerprint B is given by integrating the density of minutiae in A in a tolerance region around p. The

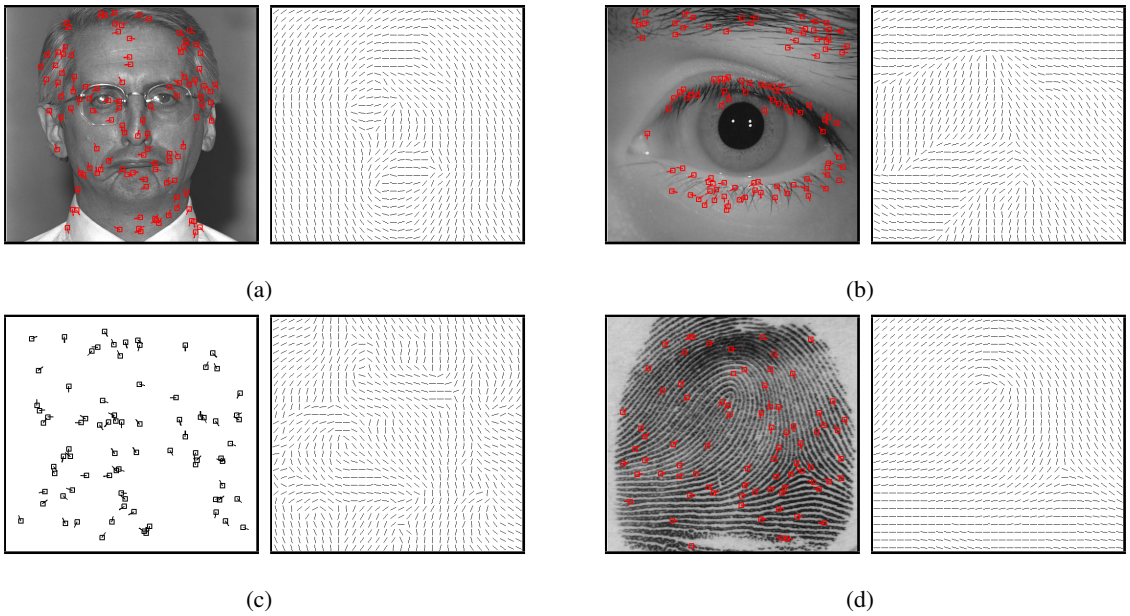

Fig. 18. Validating a minutiae pattern at the orientation field level. (a) Minutiae extracted from a face image and the orientation field reconstructed from the minutiae, (b) minutiae extracted from an iris image and the orientation field reconstructed from the minutiae, (c) a synthetic minutiae pattern following the uniform model and the orientation field reconstructed from the minutiae, (d) the minutiae pattern of a true fingerprint image (NIST SD4, F1887) and the orientation field reconstructed from the minutiae.

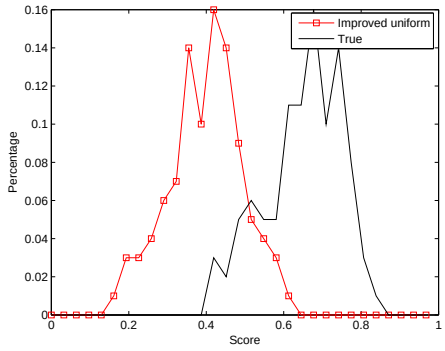

Fig. 19. Distributions of validity scores at the minutia level for minutiae patterns simulated by the improved uniform model and true minutiae patterns.

justification for treating each minutia equally in computing the match score is that the minutiae follow a uniform distribution model [13]. Thus the probability that any minutia in A has a matched minutia in B is the same. In other words, no minutia is more distinctive than any other. However, according to our minutiae model, the higher the density of a minutia, the more

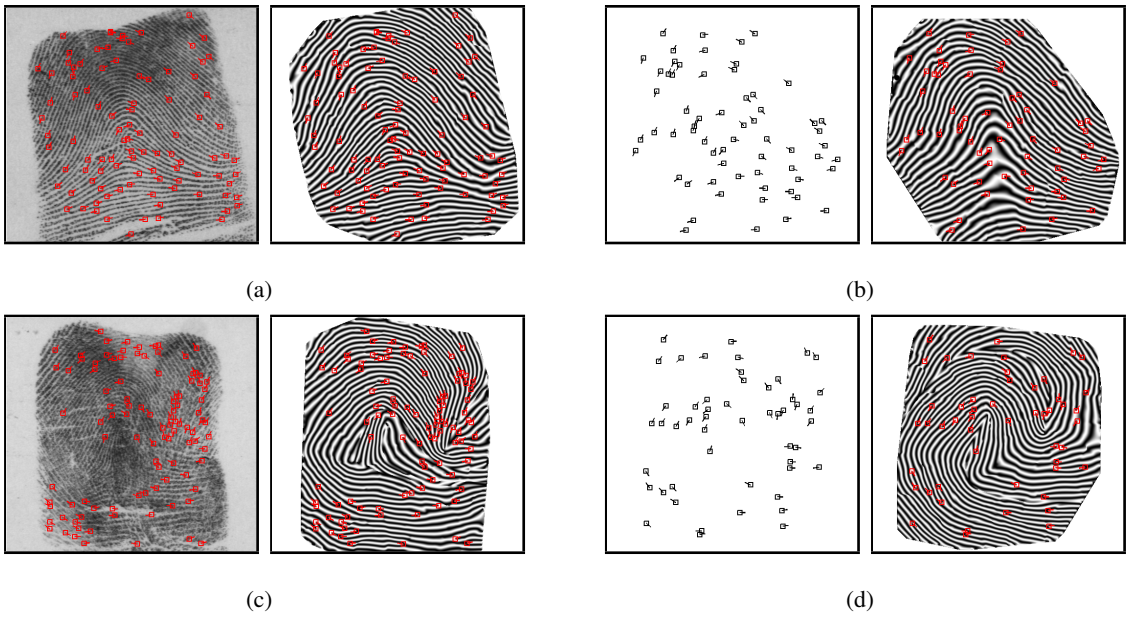

Fig. 20. Validating a minutiae pattern at the minutiae level. (a) A true minutiae pattern (NIST SD4, F1885) and the image reconstructed from it, (b) a synthetic minutiae pattern (with the same orientation field as (a)) simulated using the improved uniform model and the image reconstructed from it, (c) a true minutiae pattern (NIST SD4, F0844) and the image reconstructed from it, (d) a synthetic minutiae pattern (with the same orientation field as (c)) simulated using the improved uniform model and the image reconstructed from it. The validity score of the true minutiae pattern in (a) is larger than that of the synthetic minutiae pattern in (b), while the validity score of the true minutiae pattern in (c) is smaller than that of the synthetic minutiae pattern in (d) due to many missing and spurious minutiae in (c).

probable it is that it has a matched minutia. In other words, minutiae in large density area are less distinctive than minutiae in low density area.

Minutia distinctiveness can be utilized in computing the match score as follows. Let n be the number of minutiae within R pixels from a minutia p. The weight or distinctiveness associated with p is defined as:

$$w = \exp(-\frac{n}{N(R)}), \tag{19}$$

where $N(R)$ denotes the average number of neighboring minutiae within R pixels from any minutia. For $R = 40$ pixels, $N(R)$ is found to be around 3 on a set of training fingerprints. The match score is computed as the sum of the weight of each matched minutia.

To validate this approach, we use the Hough transform based minutiae matcher [37] to find matched minutiae for all 2,800 genuine and 4,950 impostor matches in FVC2002 DB1_A. Figure 21 shows the ROC curves of two match score computation methods, namely, the number of

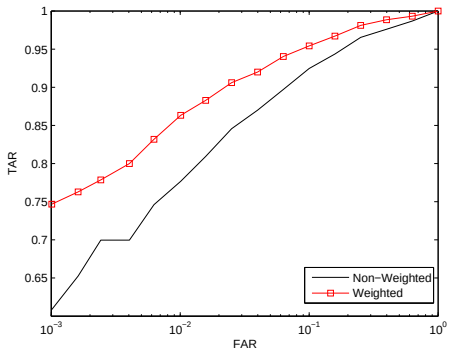

Fig. 21. ROC curves of two scoring methods (weighted and non-weighted matched minutiae) on FVC2002 DB1_A. A total of 2,800 genuine matches and 4,950 impostor matches are performed.

matched minutiae pairs and the weighted matched minutiae pairs. This figure indicates that the weighted score is better than the unweighted score in discriminating genuine from impostor matches. Note that the purpose of this experiment is to show the relative contribution of minutia distinctiveness rather than to develop a new fingerprint matcher. A higher match accuracy can be obtained by using more sophisticated matching algorithms and including additional features [7], [38]. Figure 22 shows an example to illustrate why the weighted score has a higher discriminative ability than the unweighted score. In this example, although the impostor fingerprint pair contains a larger number of matched minutiae than the genuine fingerprint pair, the weighted score of the genuine pair is larger because the matched minutiae in the genuine pair are more distinctive.

The above experiment indicates that both the number of matched minutiae pairs and the distinctiveness of minutiae affect the strength of a match. Thus the standard for identification that requires a minimum number of matched minutiae between a latent and a known print may not be the best choice [1]. This experiment also suggests that fingerprint individuality study should not pose the individuality problem as simply estimating the probability that two arbitrary minutiae sets share m minutiae, as done in [13], [14].

VI. Conclusion and Future Work

Although automatic fingerprint recognition technology has advanced significantly in the past forty years, a fundamental problem, namely, probabilistic distribution of fingerprint patterns, has yet to be solved. Statistical modeling of fingerprints is of fundamental importance for many

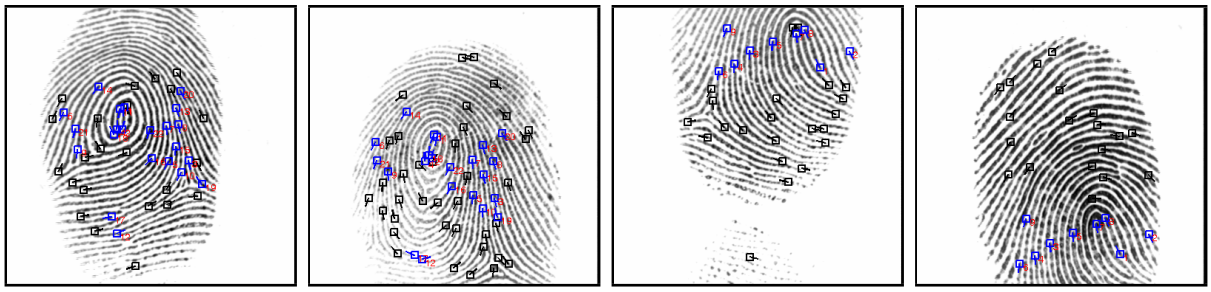

(a) (b)

Fig. 22. Although the impostor pair in (a) has 22 matched minutiae pairs and the genuine pair in (b) has only 9 matched minutiae pairs, the weighted score of the genuine pair is 8.1, larger than the weighted score of the impostor pair, 7.4. The matched minutiae are shown in blue color while the unmatched minutiae are shown in black color.

problems in fingerprint recognition, varying from synthesis, feature extraction, to individuality assessment. Considering the distinctiveness and popularity of minutiae-based representation of fingerprints, we focus our study on the problem of statistical modeling of minutiae patterns. We use a two level generative model to approximate the statistics of minutiae patterns, with the first level approximating the distribution of orientation fields and the second level modeling the distribution of minutiae location and polarity. We have also proposed a minutiae-based fingerprint reconstruction algorithm that preserves the given minutiae pattern and applied it to evaluate the proposed minutiae model and two previously published minutiae models; fingerprints reconstructed from minutiae simulated using the proposed model are more realistic than minutiae simulated by other models. We have applied the proposed model to address two specific problems: (i) recognizing non-fingerprint patterns and (ii) using minutia distinctiveness in match score computation. Use of the proposed model provides improved results for both the problems.

The current study can be continued along the following directions. We have assumed minutiae to be independent of each other. In practice, minutiae with different polarities tend to appear in pair. We plan to improve the statistical model of minutiae to take into account possible interaction between neighbouring minutiae. Another interesting problem is to apply the minutiae model to other practical problems such as individuality estimation and altered fingerprint detection.

ACKNOWLEDGMENT

Portions of the research in this paper use the FVC2002 database (collected by the Biometric Systems Lab at University of Bologna), the NIST SD4 and FERET databases (collected by the

NIST), and the CASIA-IrisV3 database (collected by the Chinese Academy of Sciences' Institute of Automation (CASIA)). This work was supported by the National 863 Hi-Tech Development Program of China under Grant 2008AA01Z123, and the National Natural Science Foundation of China under Grants 60805017, 61005023, and 61020106004. Part of Anil Jain's research was supported by WCU (World Class University) program through the National Research Foundation of Korea funded by the Ministry of Education, Science and Technology (R31-2008-000-10008-0) to Korea University.

REFERENCES

[1] C. Champod, C. Lennard, P. Margot, and M. Stoilovic, *Fingerprints and Other Ridge Skin Impressions*. CRC Press, 2004.

[2] D. Maltoni, D. Maio, A. K. Jain, and S. Prabhakar, *Handbook of Fingerprint Recognition*, 2nd ed. Springer-Verlag, 2009.

[3] Q. Xiao and H. Raafat, "Fingerprint Image Postprocessing: Combined Statistical and Structural Approach," *Pattern Recognition*, vol. 24, no. 10, pp. 985–992, 1991.

[4] J. Feng, A. K. Jain, and A. Ross, "Detecting Altered Fingerprints," in *Proc. 20th International Conference on Pattern Recognition*, 2010, pp. 1622–1625.

[5] D. A. Stoney, "Measurement of Fingerprint Individuality," in *Advances in Fingerprint Technology*, 2nd ed., H. C. Lee and R. E. Gaensslen, Eds. CRC Press, 2001, pp. 327–388.

[6] R. Cappelli, "Synthetic Fingerprint Generation," in *Handbook of Fingerprint Recognition*, 2nd ed., D. Maltoni, D. Maio, A. K. Jain, and S. Prabhakar, Eds. Springer-Verlag, 2009.

[7] J. Feng, "Combining Minutiae Descriptors for Fingerprint Matching," *Pattern Recognition*, vol. 41, no. 1, pp. 342–352, 2008.

[8] N. K. Ratha, S. Chikkerur, J. H. Connell, and R. M. Bolle, "Generating Cancelable Fingerprint Templates," *IEEE Transactions on Pattern Analysis and Machine Intelligence*, vol. 29, no. 4, pp. 561–572, 2007.

[9] A. Nagar and A. K. Jain, "On the Security of Non-invertible Fingerprint Template Transforms," in *Proc. First IEEE International Workshop on Information Forensics and Security*, 2009, pp. 81–85.

[10] A. Ross, J. Shah, and A. K. Jain, "From Template to Image: Reconstructing Fingerprints from Minutiae Points," *IEEE Transactions on Pattern Analysis and Machine Intelligence*, vol. 29, no. 4, pp. 544–560, 2007.

[11] R. Cappelli, A. Lumini, D. Maio, and D. Maltoni, "Fingerprint Image Reconstruction from Standard Templates," *IEEE Transactions on Pattern Analysis and Machine Intelligence*, vol. 29, no. 9, pp. 1489–1503, 2007.

[12] J. Feng and A. K. Jain, "Fingerprint Reconstruction: From Minutiae to Phase," *IEEE Transactions on Pattern Analysis and Machine Intelligence*, vol. 33, no. 2, pp. 209–223, 2011.

[13] S. Pankanti, S. Prabhakar, and A. K. Jain, "On the Individuality of Fingerprints," *IEEE Transactions on Pattern Analysis and Machine Intelligence*, vol. 24, no. 8, pp. 1010–1025, 2002.

[14] Y. Zhu, S. C. Dass, and A. K. Jain, "Statistical Models for Assessing the Individuality of Fingerprints," *IEEE Transactions on Information Forensics and Security*, vol. 2, no. 3, pp. 391–401, 2007.

[15] Y. Chen and A. K. Jain, "Beyond Minutiae: A Fingerprint Individuality Model with Pattern, Ridge and Pore Features," in *Proc. Second International Conference on Biometrics*, 2009, pp. 523–533.

[16] K. G. Larkin and P. A. Fletcher, "A Coherent Framework for Fingerprint Analysis: Are Fingerprints Holograms?" *Optics Express*, vol. 15, pp. 8667–8677, 2007.

[17] B. G. Sherlock and D. M. Monro, "A Model for Interpreting Fingerprint Topology," *Pattern Recognition*, vol. 26, no. 7, pp. 1047–1055, 1993.

[18] J. Zhou and J. Gu, "Modeling Orientation Fields of Fingerprints with Rational Complex Functions," *Pattern Recognition*, vol. 37, no. 2, pp. 389–391, 2004.

[19] S. Huckemann, T. Hotz, and A. Munk, "Global Models for the Orientation Field of Fingerprints: An Approach Based on Quadratic Differentials," *IEEE Transactions on Pattern Analysis and Machine Intelligence*, vol. 30, no. 9, pp. 1507–1519, 2008.

[20] D. C. Ghiglia and M. D. Pritt, *Two-Dimensional Phase Unwrapping: Theory, Algorithms, and Software*. New York: John Wiley and Sons, 1998.

[21] D. J. Bone, "Fourier Fringe Analysis: the Two-Dimensional Phase Unwrapping Problem," *Applied Optics*, vol. 30, no. 25, pp. 3627–3632, 1991.

[22] A. K. Jain and J. Feng, "Latent Fingerprint Matching," *IEEE Transactions on Pattern Analysis and Machine Intelligence*, vol. 33, no. 1, pp. 88–100, 2011.

[23] M. Indovina and A. Hicklin, "ELFT-EFS – NIST Evaluation of Latent Fingerprint Technologies: Extended Feature Sets Evaluation #1," NIST, Tech. Rep., January 2010.

[24] M. Kücken and A. C. Newell, "Fingerprint Formation," *Journal of Theoretical Biology*, vol. 235, no. 1, pp. 71–83, 2005.

[25] H. Cummins and M. Midlo, *Finger Prints, Palms and Soles: An Introduction to Dermatoglyphics*. Dover Publications, 1961.

[26] NIST Special Database 14, NIST Mated Fingerprint Card Pairs 2 (MFCP2).

[27] R. Cappelli and D. Maltoni, "On the Spatial Distribution of Fingerprint Singularities," *IEEE Transactions on Pattern Analysis and Machine Intelligence*, vol. 31, no. 4, pp. 742–748, 2009.

[28] J. Illian, A. Penttinen, H. Stoyan, and D. Stoyan, *Statistical Analysis and Modelling of Spatial Point Patterns*. John Wiley & Sons, Inc., 2008.

[29] B. D. Ripley, *Stochastic Simulation*. John Wiley & Sons, Inc., 1987.

[30] ——, "Modelling Spatial Patterns," *Journal of the Royal Statistical Society. Series B (Methodological)*, vol. 39, no. 2, pp. 172–212, 1977.

[31] E. Tabassi, C. Wilson, and C. Watson, "Fingerprint Image Quality," NISTIR 7151, August 2004.

[32] FERET Database, http://www.itl.nist.gov/iad/humanid/feret/.

[33] CASIA Iris Image Database, http://biometrics.idealtest.org/.

[34] Neurotechnology Inc., VeriFinger, http://www.neurotechnology.com.

[35] A. K. Jain, L. Hong, and R. M. Bolle, "On-line Fingerprint Verification," *IEEE Transactions on Pattern Analysis and Machine Intelligence*, vol. 19, no. 4, pp. 302–314, 1997.

[36] A. M. Bazen and S. H. Gerez, "Fingerprint Matching by Thin-Plate Spline Modelling of Elastic Deformations," *Pattern Recognition*, vol. 36, no. 8, pp. 1859–1867, August 2003.

[37] N. K. Ratha, K. Karu, S. Chen, and A. K. Jain, "A Real-Time Matching System for Large Fingerprint Databases," *IEEE Transactions on Pattern Analysis and Machine Intelligence*, vol. 18, no. 8, pp. 799–813, 1996.

[38] X. Chen, J. Tian, and X. Yang, "A New Algorithm for Distorted Fingerprints Matching Based on Normalized Fuzzy Similarity Measure," *IEEE Transactions on Image Processing*, vol. 15, no. 3, pp. 767–776, 2006.